PROCEEDINGS OF SCIENCE

Latest results from the MEG experiment and the MEG II upgraded detector

A. M. Baldini[*†]
INFN Sezione di Pisa
E-mail: alessandro.baldini@pi.infn.it

We present the analysis results of about one half of the data collected by the MEG experiment at the Paul Scherrer Institut (corresponding to 3.6×10^{14} muons stopped on target) with improved analysis algorithms. The data show no excess of events compared to background expectations and yield a new upper limit on the branching ratio of this decay of 5.7×10^{-13} (90% confidence level). This represents a four times more stringent limit than the previous world best limit set by MEG. The experiment stopped data taking at the end of August 2013. We describe the future plans for a second phase (MEG II) of the experiment

XV Workshop on Neutrino Telescopes,
11-15 March 2013
Venice, Italy

[*]Speaker.
[†]On behalf of the MEG collaboration

PoS(Neutel 2013)035

1. Introduction

Despite the existence of neutrino oscillations, the Lepton Flavor Violating (LFV) $\mu \to e\gamma$ decay is predicted to have an unobservable low rate within the Standard Model of elementary particles physics (SM) [1]. Conversely several new physics models [2, 3, 4, 5] beyond SM (BSM), particularly after the recent measurements of a large θ_{13} at reactor [6, 7, 8] and accelerator [9] experiments, predict measurable rates for this decay. An observation of the $\mu \to e\gamma$ decay would hence represent an unambiguous sign of BSM physics while improvements in the branching ratio decay limit constitute significant constraints, complementary to those obtainable at high energy colliders, of the parameter space of such BSM models

The MEG detector[10] is composed of a positron spectrometer formed by a set of drift chambers (DC) and scintillation timing counters (TC) located inside a superconducting solenoid with a gradient field along the beam axis (1.27 T at the center and 0.49 T at either end) and a photon detector, located outside of the solenoid, made of a homogeneous volume (900 ℓ) of liquid xenon (LXe) viewed by 846 UV-sensitive photomultipliers (PMTs) submerged in the liquid.

The MEG detector response, resolutions and stability are constantly monitored and calibrated by a multi-element calibration system which, among other items, includes a Cockroft-Walton (CW) proton accelerator to excite nuclear reactions with photons, the $\pi^- p \to \pi^0 n$ charge exchange reaction (CEX) and a recently developed polyethylene target, to be used in alternative to the muon stopping target, for the Mott scattering of a monochromatic positron beam.

2. The new analysis algorithms

In each event positron and photon candidates are characterized by five observables, the γ-ray and e^+ energies (E_γ, E_e), their relative directions ($\theta_{e\gamma}$, $\phi_{e\gamma}$ [11]) and emission time ($t_{e\gamma}$).

The positron track is reconstructed by combining its measured positions at each DC layers (hits) in the spectrometer. The positron kinematic variables are extracted with a Kalman filter track fit technique [12]. This algorithm was completely revised, including a better model for the hits and the track itself, based on the GEANE package [13]: an improved model for the detector material is included to account for multiple scattering and energy loss and for the non-uniform magnetic field, that is measured with a 0.2% accuracy. The positron track is then propagated to the target and to the TC with an iterative refinement of the hits using the constraint given by the target plane and size and by the positron time measurement.

The track fit yields a parameters covariance matrix that results to be in very good agreement with the measured resolutions: those are extracted in a sample of tracks with two full turns in the DC, by comparing the track parameters determined independently for each turn. Therefore this per-track error estimate allows to follow the variable DC performance during the data-taking periods. It provides an additional input to the maximum likelihood analysis.

The overall improvement in positron reconstruction with respect to the previous data analysis is shown in Fig.1 (Left) where the reconstructed Michel decays spectrum near the kinematic edge shows a reduced tail. The energy resolution is evaluated by fitting this kinematic edge and is well described by a sum of three Gaussian curves with a resolution of 305 keV for the core (85%) component.

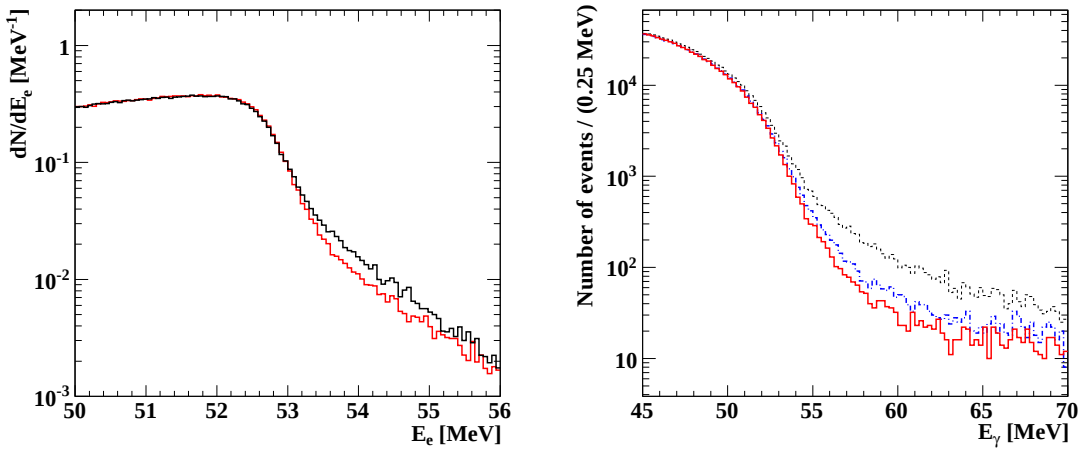

Figure 1: (Left) The positron Michel spectrum in the same sideband dataset with the old (dark) and the new (light) track reconstruction code. (Right) The γ-ray background spectra from the sidebands of the physics data in 2010 with different pile-up elimination algorithms: the black dot histogram shows the spectrum without pile-up elimination, the blue dot-dashed one that obtained with the previous algorithm, and the red solid one that obtained with the new algorithm

The LXe detector uses the xenon scintillation light to measure the total energy released by the photon, the position and time of its first interaction. The reconstruction of the γ-ray energy is based on the weighted sum of the number of photons detected by all PMTs. Monochromatic 55 MeV γ-rays from π^0 decays are used to determine the absolute energy scale, while spatial non-uniformities of the energy reconstruction are corrected by using both 17.6 MeV γ-rays from CW run and the 55 MeV γ-rays.

It is important to identify and unfold photon pile-up events at high muon rates since at $3 \times 10^7 \mu^+$/s beam rate, around 15% of triggered events suffer from pile-up. For the previously published analyses, photon pile-up events were identified topologically by the pattern of PMT light distribution and temporally by the leading edge time distribution in the time reconstruction, without the use of detailed waveform information. In addition to these methods, a new algorithm, analyzing waveforms after summing up all channels at the end of the full chain of photon reconstruction, was developed. It enables the efficient identification and removal of pile-up photons by using template waveforms. Consequently the charge integration window for the energy estimate is re-adjusted, resulting in a better energy reconstruction. This improvement is shown in Fig. 1 (Right) where we compare the photon energy spectra obtained with different pile-up elimination algorithms. The reduced tail in the high energy region is clearly visible. The efficiency of photon reconstruction is improved from 59% to 63% due to the new algorithm.

3. Analysis results

The previous best upper limit on the $\mu^+ \to e^+\gamma$ decay branching ratio $\mathscr{B}$ ($\mathscr{B} < 2.4 \times 10^{-12}$ at 90% C.L.) was set by the MEG experiment [14] with an analysis of the data taken in the years 2009–2010, for a total number of 1.75×10^{14} positive muons stopped on target.

We present here an updated analysis of the 2009–2010 data sample, based on the previously described improved algorithms for the reconstruction of positrons and photons together with the analysis of the data sample collected in 2011 with a beam intensity of $3 \times 10^7 \mu^+/\mathrm{s}$, which corresponds to 1.85×10^{14} stopped muons on target. Furthermore the combined analysis of the full 2009–2011 statistics is presented.

The signature of the signal event is given by a back-to-back, monoenergetic, time coincident photon-positron pair from the two body $\mu^+ \to e^+\gamma$ decay. In each event, positron and photon candidates are described by five observables: the photon and positron energies (E_γ, E_e), their relative directions ($\theta_{e\gamma}$, $\phi_{e\gamma}$) [11] and emission time ($t_{e\gamma}$). Our analysis is based on a maximum likelihood technique applied in the analysis region defined by $48 < E_\gamma < 58\,\mathrm{MeV}$, $50 < E_e < 56\,\mathrm{MeV}$, $|t_{e\gamma}| < 0.7\,\mathrm{ns}$, $|\theta_{e\gamma}| < 50\,\mathrm{mrad}$ and $|\phi_{e\gamma}| < 50\,\mathrm{mrad}$, which is described in detail in [14]. We call "time sidebands" the regions in the variable space defined by $1 < |t_{e\gamma}| < 4\,\mathrm{ns}$, "$E_\gamma$-sideband" that defined by $40 < E_\gamma < 48$ MeV and "angle sidebands" those defined by $50 < |\phi_{e\gamma}| < 150\,\mathrm{mrad}$ or $50 < |\theta_{e\gamma}| < 150\,\mathrm{mrad}$.

A blind analysis procedure is applied only to the new dataset in 2011 by masking a region of $48 < E_\gamma < 58\,\mathrm{MeV}$ and $|t_{e\gamma}| < 1\,\mathrm{ns}$ until the Probability Density Functions (PDFs) for the likelihood function are finalized. For all the datasets including 2009–2010 data the background studies and the extraction of the PDFs are carried out in the time and angle sidebands. The maximum likelihood fit is performed in order to estimate the number of signal and background events in the analysis region. The definition of the likelihood function is described in detail in [14]. All PDFs as a function of the observables are extracted from the data.

The sensitivity ($\mathscr{S}_{90}$) is estimated as the median of the distribution of the branching ratio upper limits at 90% C.L., calculated over an ensemble of pseudo-experiments, randomly generated according to the PDFs based on a null signal hypothesis, with the background rate evaluated from the sidebands. The sensitivities have been so evaluated for the 2009–2010 combined data, the 2011 data alone and the 2009–2011 combined data sample, and are reported in Table 1.

Table 1: Best fit values ($\mathscr{B}_{\mathrm{fit}}$'s), branching ratios ($\mathscr{B}_{90}$) and sensitivities ($\mathscr{S}_{90}$)

Dataset	$\mathscr{B}_{\mathrm{fit}} \times 10^{12}$	$\mathscr{B}_{90} \times 10^{12}$	$\mathscr{S}_{90} \times 10^{12}$
2009–2010	0.09	1.3	1.3
2011	−0.35	0.67	1.1
2009–2011	−0.06	0.57	0.77

Figure 2 shows the event distributions in the (E_e, E_γ)- and $(\cos\Theta_{e\gamma}, t_{e\gamma})$-planes for the combined 2009–2011 dataset, where $\Theta_{e\gamma}$ is the opening angle between positron and photon, together with the

contours of the averaged signal PDFs.

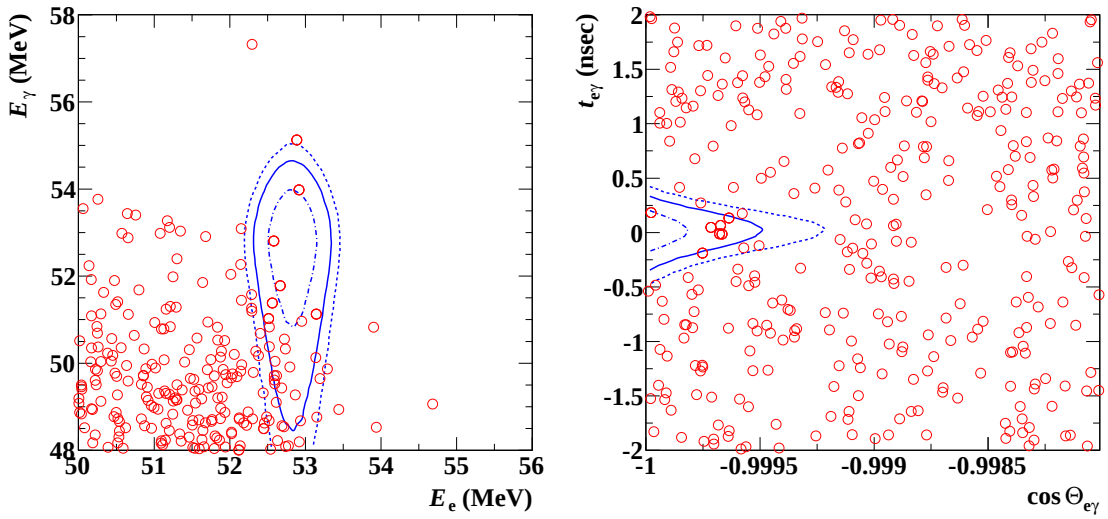

Figure 2: Event distributions for the combined 2009–2011 dataset in the (E_e, E_γ)- and $(\cos\Theta_{e\gamma}, t_{e\gamma})$-planes. In the top (bottom) panel, a selection of $|t_{e\gamma}| < 0.244$ ns and $\cos\Theta_{e\gamma} < -0.9996$ with 90% efficiency for each variable ($52.4 < E_e < 55$ MeV and $51 < E_\gamma < 55.5$ MeV with 90% and 74% efficiencies for E_e and E_γ, respectively) is applied. The signal PDF contours (1, 1.64 and 2 σ) are also shown.

The observed profile likelihood ratios as a function of the branching ratio are shown in Fig. 3. The best $\mathscr{B}$ estimates, upper limits at 90% C.L. ($\mathscr{B}_{90}$) and $\mathscr{S}_{90}$ for the combined 2009–2010 dataset, the 2011 data alone and the total 2009–2011 dataset are listed in Table 1. The $\mathscr{B}_{90}$ for the latter is 5.7×10^{-13}.

4. MEG II

Since, as it is clear from Figure 2, the background extends in the signal region, the sensitivity of the experiment is not going to linearly increase with statistics. For this reason the data taking of the first phase of the MEG experiment was stopped at the end of August 2013; the total statistics corresponding to about twice that analysed for this talk. We estimate to reach a final sensitivity to the $\mu^+ \to e^+\gamma$ decay branching ratio $\mathscr{B}$ around $4 \div 5 \times 10^{-13}$ by analysing the full MEG data sample.

The proposal of an upgraded MEG detector for a phase II of the experiment[15] was approved by PSI on January 2013 and fully financed by the different funding agencies.

The key features of MEG II , aimed at improving the experimental sensitivity down to $\mathscr{B} \sim 6 \times 10^{-14}$, are to increase the rate capability of all detectors to enable running at the full PSI beam intensity ($\sim 10^8 \mu^+/\text{s}$), while also improving the energy and angular and timing resolutions, for both the positron and photon arms of the detector. This is especially valid on the positron-side, where a new low-mass, single volume, high granularity tracker is under development. This, in combination with a thinner stopping target and hence a reduction in the multiple scattering of the positrons, will lead to the spatial, angular and energy requirements being met on the positron side.

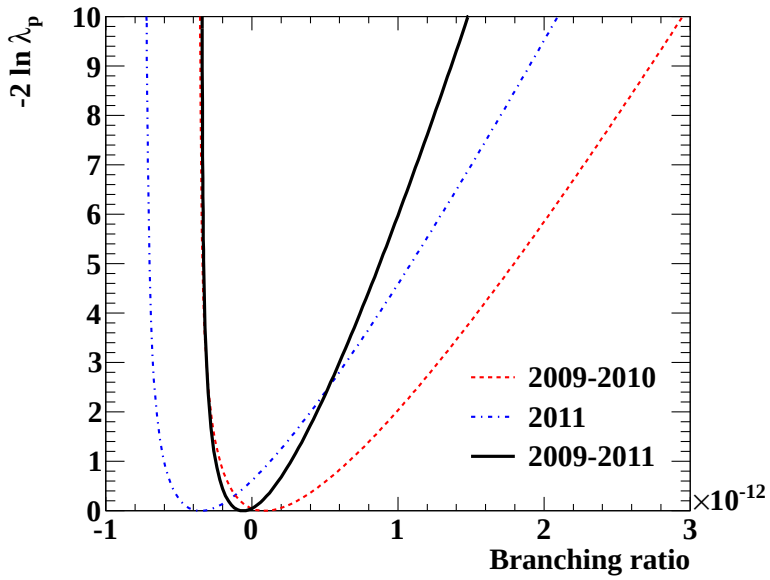

Figure 3: Observed profile likelihood ratios (λ_p) as a function of the branching ratio for the 2009–2010 combined data, the 2011 data alone and the combined 2009–2011 data sample.

A new highly segmented, fast timing counter array will replace the old system, so allowing improved timing resolution capabilities in order to minimize the number of background events entering the signal timing window. The photon-arm will also be improved by increasing the granularity at the incident face of the LXe detector, by replacing the current photomultiplier tubes (PMTs) with a larger number of smaller photosensors and optimizing the photosensor layout also on the lateral faces. This should also lead to improved energy and spatial resolutions for the LXe detector. Finally, in order to meet the stringent requirements of an increased number of readout channels and to cope with the necessary bandwidth required by such a system, a new DAQ scheme involving the implementation of a new combined readout board capable of integrating the various functions of digitization, trigger capability and splitter functionality into one condensed unit, is also under development.

The schedule foresees to have the MEG II detector ready within 2015 and to run the experiment at the full PSI beam intensity in the years 2016-2018.

References

[1] S.T. Petcov, Sov. J. Nucl. Phys. **25** (1977) 340

[2] R. Barbieri, L. Hall and A. Strumia, Nucl. Phys. B **455** (1995) 219.

[3] J. Hisano, D. Nomura and T. Yanagida, Phys. Lett. B **437** (1998) 351.

[4] M. Raidal *et al.*, Eur. Phys. J. C **57** (2008) 13.

[5] G. Blankenburg *et al.*, Eur. Phys. J. C **72** (2012) 2126.

[6] F.P. An *et al.*, Phys. Rev. Lett. **108** (2012) 171803.

[7] J.K. Ahn *et al.*, Phys. Rev. Lett. **108** (2012) 191802.

[8] Y. Abe *et al.*, arXiv:1301.2948 [hep-ex].

[9] K. Abe *et al.*, Phys. Rev. Lett. **107** (2011) 041801.

[10] Eur. Phys. J. C **73** (2013) 2365.

[11] $\theta_{e\gamma} = (\pi - \theta_e) - \theta_\gamma$ and $\phi_{e\gamma} = (\pi + \phi_e) - \phi_\gamma$, θ and ϕ being the polar angle and the azimuthal angle, respectively, taking the z-axis as the beam-axis.

[12] P. Billoir, Nucl. Instrum. Meth. A 225 (1984) 352; R. Frühwirth, Nucl. Instrum. Meth. A 262 (1987) 444;

[13] V. Innocente and E. Nagy, Nucl. Instrum. Meth. A 324 (1993) 297; A. Fontana et al. J. Phys. Co nf. Ser. 119 (2008) 032018

[14] J. Adam *et al.*, Phys. Rev. Lett. **107** (2011) 171801.

[15] A. M. Baldini *et al.*, arXiv:1301.7225v2 [physics.ins-det].